Nonlinear acoustic metamaterial for efficient frequency down-conversion

Geun Ju Jeon and Joo Hwan Oh[*]

School of Mechanical, Aerospace and Nuclear Engineering, Ulsan National Institute of Science and Technology,
UNIST-gil 50, Eonyang-eup, Ulju-gun, Ulsan 44919, Korea

Frequency conversion is one of the most important nonlinear wave phenomena that has been widely used in the field of electromagnetic waves for changing signal frequencies. Recently, studies on frequency conversion have been actively performed in the field of acoustics owing to its importance in nonlinear ultrasonic nondestructive evaluation and directional speakers. However, acoustic frequency conversion presents relatively poor efficiency owing to the small amplitudes of the converted frequencies and undesired intermodulation. Herein, we propose an acoustic metamaterial to achieve an efficient frequency down-conversion of acoustic waves. Based on background theory, we discovered that the amplitudes of the converted frequencies are inversely proportional to the cube of the speed of sound. Accordingly, we amplify the converted frequency components by reducing the effective speed of sound by coiling up space while suppressing undesired intermodulation by the Bragg gap. Numerical simulation and analytical results show that efficient frequency down-conversion is possible using the corresponding metamaterial. Additionally, dissipation due to viscosity and boundary layer effects is considered. We expect our study results to facilitate research regarding acoustic frequency conversion.

I. INTRODUCTION

Frequency conversion is a nonlinear wave phenomenon that provides waves with the desired frequency from incident waves having different frequencies. The most widely used method in frequency conversion is to add a modulating wave (with frequency f_2) to an incident wave (with frequency f_1) in nonlinear media. Owing to the nonlinear effect, waves with a frequency of $f_1 + f_2$ or $|f_1 - f_2|$ can be generated. Hence, by appropriately selecting the frequency of the modulating wave f_2, one can achieve the frequency conversion corresponding to the frequency of $f_1 + f_2$ or $|f_1 - f_2|$. In general, achieving the frequency of $f_1 + f_2$ is known as frequency up-conversion, whereas that of $|f_1 - f_2|$ is known as frequency down-conversion. Because the desired frequency can be easily and actively achieved, the frequency up- and down-conversion has been widely used in the field of electromagnetic waves, enabling various new techniques [1]. The radio frequency (rf) → intermediate frequency (i.f.) conversion of the superheterodyne receiver is a representative example. In addition to rf communication, frequency conversion has been widely used in the telecommunications field, in applications such as radio transmitters, television receivers, and optical modulators.

Based on advances in electromagnetic waves, research regarding frequency conversion has recently been expanded to the field of acoustic waves, e.g., directional loudspeakers and nondestructive evaluation [2–7]. As frequency conversion has enabled the development of a new field in electromagnetic waves, acoustic frequency conversion is expected to expand the related field. However, unlike electromagnetic frequency conversion, significant technical barriers affecting acoustic frequency conversion exist, as plotted in Fig. 1(a). The first barrier is the small amplitude of the frequency-converted waves. In general, the conventional acoustic media have a small nonlinear parameter [8]. Hence, frequency conversion with conventional acoustic media only provides a small number of converted waves. This is more critical for the frequency down-conversion case, which is closely associated with various applications such as directional loudspeakers. The second barrier is undesired intermodulation, in which not only desired frequency waves but also various undesired frequency waves are generated by the frequency conversion. To achieve efficient frequency conversion, undesired frequency waves should be filtered out [4]. For nonlinear cases, the generated undesired frequency waves may regenerate other undesired frequency waves. Hence, signal processing, filtering undesired frequency waves after the conversion, is insufficient; suppression of the undesired frequency waves should be introduced, although this is impossible with signal processing.

To overcome these barriers, recent progress in artificial periodic structures, known as metamaterials, may be considered. Owing to the unit cell configuration of a metamaterial, interesting wave phenomena [9–18] have been discovered that have enabled various new wave devices. In fact, metamaterials have been actively applied to nonlinear electromagnetic cases. For instance, enhancing the nonlinear effect using slow waves from metamaterials has been actively investigated [19–24]. By utilizing the metamaterial's internal resonance or band gap phenomenon [19,20], the wave's group velocity can be decelerated, causing the wave energy to be spatially compressed. Consequently, the light-matter interaction becomes more active, and the nonlinear effect can be improved by using the metamaterials [19]. However, in acoustic waves,
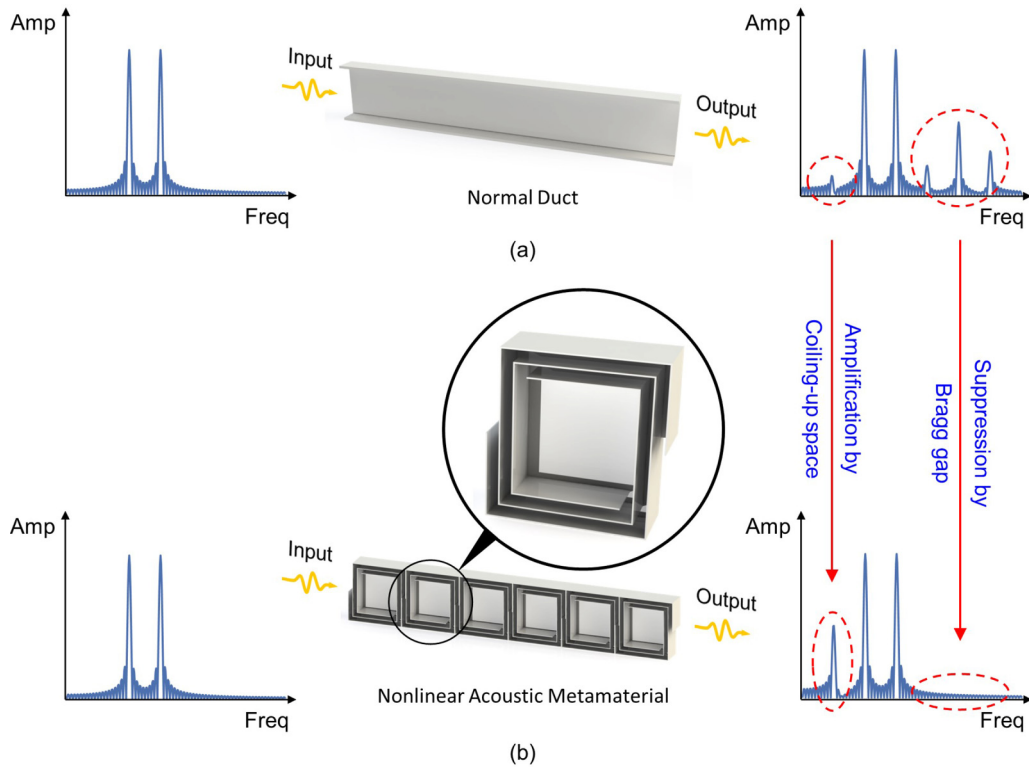
*joohwan.oh@unist.ac.kr

FIG. 1. Incident waves and transmitted waves for (a) normal duct, (b) metamaterial.

the nonlinear effect is governed by a completely different equation compared with electromagnetic waves. Therefore, an alternative metamaterial approach based on the acoustic nonlinear equation should be developed. In addition, because the undesired intermodulation is not negligible for the acoustic case as explained, this metamaterial approach should include the suppression of undesired intermodulation.

Herein, an acoustic metamaterial that can overcome the current technical barriers in acoustic frequency conversion is proposed. As explained, that the acoustic nonlinear effect is governed by a different equation compared with previous studies regarding the electromagnetic nonlinear effect should be considered. Therefore, we applied the Westervelt equation [2,25], i.e., one of the general acoustic wave equations describing nonlinearities, to design the metamaterial. Using the perturbation method [26], we discovered that the frequency conversion was inversely proportional to the density and cube of the wave speed of the nonlinear media. In other words, the amplitude of the frequency-converted waves can be increased using a nonlinear acoustic metamaterial whose wave speed is extremely low but whose effective density is small. This indicates that resonance-based metamaterials (whose effective density goes to infinity when an extremely low wave speed is achieved) are not preferred in acoustic frequency conversion, unlike in electromagnetic cases. Therefore, we utilized the previous idea of coiling up space [27–31], as shown in Fig. 1(b), to overcome the first technical barrier.

In addition, the metamaterial shown in Fig. 1(b) is designed to suppress the formation of undesired intermodulated waves. As explained, various undesired frequency waves (such as second-harmonic waves) are generated during frequency conversion, and these waves may regenerate other undesired waves. Hence, the formation of undesired waves should be suppressed during frequency conversion, rather than filtering them out after the conversion. To achieve this suppression, we designed a metamaterial based on the periodic cavity duct array, which is equivalent to a periodic *LC* circuit. In such a configuration, the acoustic wave becomes a standing wave at a certain frequency from which the Bragg gap is formed. Hence, by controlling the cavity size, the metamaterial can be designed to achieve a Bragg gap that can eliminate the undesired frequencies; i.e., the undesired frequency waves can be suppressed by the band gap.

In addition to the metamaterial design, detailed nonlinear physics for the frequency down-conversion in the nonlinear acoustic metamaterial has been investigated. Although the idea of the coiling-up space and Bragg scattering has been actively investigated, previous studies have generally focused on linear acoustics. On the other hand, because the present study mainly addresses the combined system of the nonlinear acoustic frequency conversion and the acoustic metamaterial, various related physics that were underused in the previous linear cases were investigated. First, the effective parameter of the coiling-up space metamaterial and Westervelt equation were investigated to determine the detailed physics concerning the frequency conversion. Based on our investigation, we discovered that the coiling-up space exhibited an "increased density effect," which adversely affected the frequency conversion. In addition, we discovered an important factor of "the multifrequency Fabry-Perot resonance effect" in the nonlinear acoustic metamaterial with frequency conversion. With these physical findings, we established an equation that predicts the amount of frequency conversion.

The remainder of this paper is organized as follows. First, the background theory of acoustic frequency conversion is introduced. In the background theory, the second perturbation solution is obtained using the perturbation method of the Westervelt equation, assuming two waves of different frequencies simultaneously incident on the nonlinear medium. From the obtained solution, the main factors that can enhance the frequency conversion are analyzed. Second, the design process of the metamaterial is described. The design method of metamaterials is introduced, and the nonlinear physics concerning the metamaterial is investigated. Third, the numerical validation of the designed metamaterial is described. The performance of the metamaterial is validated by comparing it with that of a normal duct. In addition, the numerical simulation results are compared with the theoretical results. Fourth, the effect of dissipation in the proposed metamaterial is investigated. Finally, the conclusions are presented.

II. BACKGROUND THEORY OF THE ACOUSTIC FREQUENCY CONVERSION

We begin with the Westervelt equation, i.e., the general wave equation in nonlinear acoustics. The Westervelt equation can be written as follows [2,24]:

$$\Delta p - \frac{1}{c_0^2}\frac{\partial^2 p}{\partial t^2} + \frac{\delta}{c_0^4}\frac{\partial^3 p}{\partial t^3} = -\frac{\beta}{\rho_0 c_0^4}\frac{\partial^2 p^2}{\partial t^2}, \quad (1)$$

where Δ is the Laplacian defined as $\Delta = \nabla^2$. In Eq. (1), p, c_0, δ, β, and ρ_0 denote the pressure, wave speed, sound diffusivity, nonlinearity coefficient, and density, respectively. Assuming zero sound diffusion ($\delta = 0$) and a one-dimensional case, Eq. (1) can be reduced to

$$\frac{\partial^2 p}{\partial x^2} - \frac{1}{c_0^2}\frac{\partial^2 p}{\partial t^2} = -\frac{\beta}{\rho_0 c_0^4}\frac{\partial^2}{\partial t^2}p^2. \quad (2)$$

In Eq. (2), the left-hand side terms are the same as those in the linear acoustic wave equation, whereas the right-hand side term corresponds to the nonlinear part.

Among the various methods that could be used to solve Eq. (2), the perturbation method is generally adopted. In the perturbation approach, the perturbation is introduced with the perturbation parameter ε.

$$\frac{\partial^2 p}{\partial x^2} - \frac{1}{c_0^2}\frac{\partial^2 p}{\partial t^2} = -\frac{\varepsilon\beta}{\rho_0 c_0^4}\frac{\partial^2}{\partial t^2}p^2, \quad p = \sum_{n=1}^{\infty}\varepsilon^{n-1}p^{(n)}. \quad (3)$$

Based on the perturbation, the following equations for each order of ε can be obtained.

$$\varepsilon^0\text{order}: \frac{\partial^2 p^{(1)}}{\partial x^2} - \frac{1}{c_0^2}\frac{\partial^2 p^{(1)}}{\partial t^2} = 0,$$

$$\varepsilon^1\text{order}: \frac{\partial^2 p^{(2)}}{\partial x^2} - \frac{1}{c_0^2}\frac{\partial^2 p^{(2)}}{\partial t^2} = -\frac{\beta}{\rho_0 c_0^4}\frac{\partial^2 (p^{(1)})^2}{\partial t^2},$$

$$\vdots$$

$$\varepsilon^n\text{order}: \frac{\partial^2 p^{(n)}}{\partial x^2} - \frac{1}{c_0^2}\frac{\partial^2 p^{(n)}}{\partial t^2} = -\frac{\beta}{\rho_0 c_0^4}\frac{\partial^2 (p^{(n-1)})^2}{\partial t^2}. \quad (4)$$

In weakly nonlinear media, where acoustic frequency conversion typically occurs, the ε^2 term and the higher-order terms are significantly smaller than the ε^0 and ε^1 terms. Therefore, the ε^2 term and higher-order terms are generally ignored. Consequently, the equations can be summarized by setting $\varepsilon = 1$ as follows:

$$p(x, t) = p^{(1)} + p^{(2)}, \quad (5a)$$

$$\frac{\partial^2 p^{(1)}}{\partial x^2} - \frac{1}{c_0^2}\frac{\partial^2 p^{(1)}}{\partial t^2} = 0, \quad (5b)$$

$$\frac{\partial^2 p^{(2)}}{\partial x^2} - \frac{1}{c_0^2}\frac{\partial^2 p^{(2)}}{\partial t^2} = -\frac{\beta}{\rho_0 c_0^4}\frac{\partial^2 (p^{(1)})^2}{\partial t^2}. \quad (5c)$$

Next, we derive the solution for frequency conversion. To achieve frequency conversion, we assume that two waves of frequencies ω_1 and ω_2 and amplitudes A_1 and A_2 are actuated from $x = 0$. This can be written as the boundary condition as follows:

$$\text{at } x = 0, \quad p = A_1 \sin \omega_1 t + A_2 \sin \omega_2 t. \quad (6)$$

With this boundary condition, we consider the ε^0th-order equation shown in Eq. (5b). Here, it is clear that no nonlinear part exists. Hence, the solution for $p^{(1)}$ in Eq. (5b) is exactly the same as that of the linear case, which can be written as

$$p^{(1)} = A_1 \sin (k_1 x - \omega_1 t) + A_2 \sin (k_2 x - \omega_2 t), \quad (7)$$

where k_1 and k_2 are wave numbers defined as $k_1 = \omega_1/c_0$ and $k_2 = \omega_2/c_0$, respectively. Regarding the ε^1th-order equation, Eq. (5c) can be rewritten by substituting Eq. (7) as follows:

$$\frac{\partial^2 p^{(2)}}{\partial x^2} - \frac{1}{c_0^2}\frac{\partial^2 p^{(2)}}{\partial t^2}$$

$$= -\frac{2\beta A_1^2\omega_1^2}{\rho_0 c_0^4}\cos 2(k_1 x - \omega_1 t)$$

$$- \frac{2\beta A_2^2\omega_2^2}{\rho_0 c_0^4}\cos 2(k_2 x - \omega_2 t)$$

$$- \frac{\beta A_1 A_2(\omega_1 + \omega_2)^2}{\rho_0 c_0^4}\cos[(k_1 + k_2)x - (\omega_1 + \omega_2)t]$$

$$+ \frac{\beta A_1 A_2(\omega_1 - \omega_2)^2}{\rho_0 c_0^4}\cos[(k_1 - k_2)x - (\omega_1 - \omega_2)t]. \quad (8)$$

For the solution of Eq. (8), one can consider the following two solution forms.

$$\begin{aligned} p^{(2)} = &B_1 x \sin 2(k_1 x - \omega_1 t) \\ &+ B_2 x \sin 2(k_2 x - \omega_2 t) \\ &+ B_3 x \sin[(k_1 + k_2)x - (\omega_1 + \omega_2)t] \\ &+ B_4 x \sin[(k_1 - k_2)x - (\omega_1 - \omega_2)t], \end{aligned} \quad (9a)$$

or

$$\begin{aligned} p^{(2)} = &B_1 t \sin 2(k_1 x - \omega_1 t) \\ &+ B_2 t \sin 2(k_2 x - \omega_2 t) \\ &+ B_3 t \sin[(k_1 + k_2)x - (\omega_1 + \omega_2)t] \\ &+ B_4 t \sin[(k_1 - k_2)x - (\omega_1 - \omega_2)t]. \end{aligned} \quad (9b)$$

However, the solution form presented in Eq. (9b) diverges as time progresses, which is physically inadmissible. Hence, the solution for $p^{(2)}$ is assumed to exhibit the form shown in Eq. (9a). Substituting Eq. (9a) into Eq. (8) yields the following equations: It is noteworthy that because the entire equation is complicated, we rearranged the equations with respect to the frequency terms.

$2\omega_1$ terms:

$$4k_1 B_1 \cos 2(k_1 x - \omega_1 t)$$
$$- 4k_1^2 B_1 x \sin 2(k_1 x - \omega_1 t)$$
$$+ \frac{4\omega_1^2 B_1}{c_0^2} x \sin 2(k_1 x - \omega_1 t)$$
$$= -\frac{2\beta A_1^2 \omega_1^2}{\rho_0 c_0^4} \cos 2(k_1 x - \omega_1 t). \qquad (10a)$$

$2\omega_2$ terms:

$$4k_2 B_2 \cos 2(k_2 x - \omega_2 t)$$
$$- 4k_2^2 B_2 x \sin 2(k_2 x - \omega_2 t)$$
$$+ \frac{4\omega_2^2 B_2}{c_0^2} x \sin 2(k_2 x - \omega_2 t)$$
$$= -\frac{2\beta A_2^2 \omega_2^2}{\rho_0 c_0^4} \cos 2((k_2 x - \omega_2 t). \qquad (10b)$$

$\omega_1 + \omega_2$ terms:

$$2B_3(k_1 + k_2) \cos[(k_1 + k_2)x - (\omega_1 + \omega_2)t]$$
$$- B_3(k_1 + k_2)^2 x \sin[(k_1 + k_2)x - (\omega_1 + \omega_2)t]$$
$$+ \frac{B_3(\omega_1 + \omega_2)^2}{c_0^2} x \sin[(k_1 + k_2)x - (\omega_1 + \omega_2)t]$$
$$= -\frac{\beta A_1 A_2 (\omega_1 + \omega_2)^2}{\rho_0 c_0^4} \cos[(k_1 + k_2)x - (\omega_1 + \omega_2)t]. \qquad (10c)$$

$\omega_1 - \omega_2$ terms:

$$2B_4(k_1 - k_2) \cos[(k_1 - k_2)x - (\omega_1 - \omega_2)t]$$
$$- B_4(k_1 - k_2)^2 x \sin[(k_1 - k_2)x - (\omega_1 - \omega_2)t]$$
$$+ \frac{B_4(\omega_1 - \omega_2)^2}{c_0^2} x \sin[(k_1 - k_2)x - (\omega_1 - \omega_2)t]$$
$$= -\frac{\beta A_1 A_2 (\omega_1 - \omega_2)^2}{\rho_0 c_0^4} \cos[(k_1 - k_2)x - (\omega_1 - \omega_2)t]. \qquad (10d)$$

Equation (10) can be further reduced by introducing wave dispersion relations $k_1 = \omega_1/c_0$ and $k_2 = \omega_2/c_0$ as follows.
$2\omega_1$ terms:

$$\frac{4B_1 \omega_1}{c_0} \cos 2(k_1 x - \omega_1 t) = -\frac{2\beta A_1^2 \omega_1^2}{\rho_0 c_0^4} \cos 2(k_1 x - \omega_1 t). \qquad (11a)$$

$2\omega_2$ terms:

$$\frac{4B_2 \omega_2}{c_0} \cos 2(k_2 x - \omega_2 t) = -\frac{2\beta A_2^2 \omega_2^2}{\rho_0 c_0^4} \cos 2(k_2 x - \omega_2 t). \qquad (11b)$$

$\omega_1 + \omega_2$ terms:

$$\frac{2B_3}{c_0}(\omega_1 + \omega_2) \cos[(k_1 + k_2)x - (\omega_1 + \omega_2)t]$$
$$= -\frac{\beta A_1 A_2 (\omega_1 + \omega_2)^2}{\rho_0 c_0^4} \cos[(k_1 + k_2)x - (\omega_1 + \omega_2)t]. \qquad (11c)$$

$\omega_1 - \omega_2$ terms:

$$\frac{2B_4}{c_0}(\omega_1 - \omega_2) \cos[(k_1 - k_2)x - (\omega_1 - \omega_2)t]$$
$$= -\frac{\beta A_1 A_2 (\omega_1 - \omega_2)^2}{\rho_0 c_0^4} \cos[(k_1 - k_2)x - (\omega_1 - \omega_2)t]. \qquad (11d)$$

Consequently, coefficients B_1, B_2, B_3, and B_4 in Eq. (9a) can be obtained as follows:

$$B_1 = -\frac{\beta A_1^2 \omega_1}{2\rho_0 c_0^3}, \quad B_2 = -\frac{\beta A_2^2 \omega_2}{2\rho_0 c_0^3},$$
$$B_3 = -\frac{\beta A_1 A_2 (\omega_1 + \omega_2)}{2\rho_0 c_0^3}, \quad B_4 = \frac{\beta A_1 A_2 (\omega_1 - \omega_2)}{2\rho_0 c_0^3} \qquad (12)$$

and $p^{(2)}$ can be obtained from Eq. (12) as

$$p^{(2)} = -\frac{\beta A_1^2 \omega_1 x}{2\rho_0 c_0^3} \sin 2(k_1 x - \omega_1 t)$$
$$- \frac{\beta A_2^2 \omega_2 x}{2\rho_0 c_0^3} \sin 2(k_2 x - \omega_2 t)$$
$$- \frac{\beta A_1 A_2 (\omega_1 + \omega_2) x}{2\rho_0 c_0^3} \sin[(k_1 + k_2)x - (\omega_1 + \omega_2)t]$$
$$+ \frac{\beta A_1 A_2 (\omega_1 - \omega_2) x}{2\rho_0 c_0^3} \sin[(k_1 - k_2)x - (\omega_1 - \omega_2)t]. \qquad (13)$$

Consequently, the acoustic waves propagating through a nonlinear medium with two incident waves of frequencies ω_1 and ω_2 can be written as

$$p(x, t) = p^{(1)} + p^{(2)}$$
$$= A_1 \sin(k_1 x - \omega_1 t)$$
$$+ A_2 \sin(k_2 x - \omega_2 t)$$
$$- \frac{\beta A_1^2 \omega_1 x}{2\rho_0 c_0^3} \sin 2(k_1 x - \omega_1 t)$$
$$- \frac{\beta A_2^2 \omega_2 x}{2\rho_0 c_0^3} \sin 2(k_2 x - \omega_2 t)$$
$$- \frac{\beta A_1 A_2 (\omega_1 + \omega_2) x}{2\rho_0 c_0^3} \sin[(k_1 + k_2)x - (\omega_1 + \omega_2)t]$$
$$+ \frac{\beta A_1 A_2 (\omega_1 - \omega_2) x}{2\rho_0 c_0^3} \sin[(k_1 - k_2)x - (\omega_1 - \omega_2)t]. \qquad (14)$$

Equation (14) suggests the following important points: First, it is clear that the frequency-converted waves have an amplitude proportional to the acoustic nonlinear coefficient β, whereas it is inversely proportional to the density ρ_0 and cube of the wave speed c_0^3. This shows that the previously known "slow wave" phenomenon observed around the locally resonant metamaterial is not suitable for acoustic frequency conversion. Because the phenomenon involves an infinite density value, we must additionally consider the density to achieve a high-efficiency frequency conversion.

In addition, Eq. (14) shows that various frequency components are generated. Here, not only the frequency down-conversion wave (with frequency of $\omega_1 - \omega_2$), but also other waves (with frequencies of $\omega_1 + \omega_2$, $2\omega_1$, and $2\omega_2$) are generated. However, their amplitudes exhibit the same behavior, i.e., all of them are proportional to β and inversely proportional to ρ_0 and c_0^3. This indicates that undesired frequency waves cannot be suppressed by tailoring the material properties, and the suppression of the undesired frequency waves should be performed based on different physics.

III. ACOUSTIC METAMATERIAL FOR FREQUENCY CONVERSION

The previous theoretical analysis indicated two important points that should be considered to achieve effective acoustic frequency conversions. First, nonlinear media with an extremely low wave speed but without an extremely high density are required. In addition, undesired frequency waves, including second-harmonic waves, should be effectively suppressed. How can we solve these issues using acoustic metamaterials?

In previous studies regarding nonlinear electromagnetics, almost flat wave dispersion branches around the band gap of photonic crystals or internal resonance metamaterials have been used to achieve extremely low wave speeds. However, for acoustic cases, these approaches are not desirable because the density is involved with the frequency conversion. Although the use of internal resonance acoustic metamaterials may provide extremely low wave speeds, as in the electromagnetic case, the effective density of the internal resonance acoustic metamaterial is known to diverge to an infinite value around the resonance frequency, which is undesirable in acoustic frequency conversion. Moreover, frequency conversion involves multiple frequencies, and the use of flat group velocity around a very narrow frequency range in phononic crystals or internal resonance metamaterials is unsuitable.

Therefore, we used the concept of the coiling-up space proposed in [27], which can control the effective properties and wave speed for a broad frequency range. This can be achieved by introducing a mazelike structure. Because acoustic waves are scalar fields, waves propagate inside the mazelike structure without any dispersion. Hence, the effective wave speed can be decelerated significantly by the mazelike structure. Using these characteristics, the acoustic coiling-up space concept has been successfully applied to achieve high refractive indices, high impedances, double negativity, near-zero densities, and sound entrapment [27–31]. Furthermore, we applied the concept of coiling-up space to improve the frequency conversion effect using an extremely low wave speed, based on the Westervelt equation.
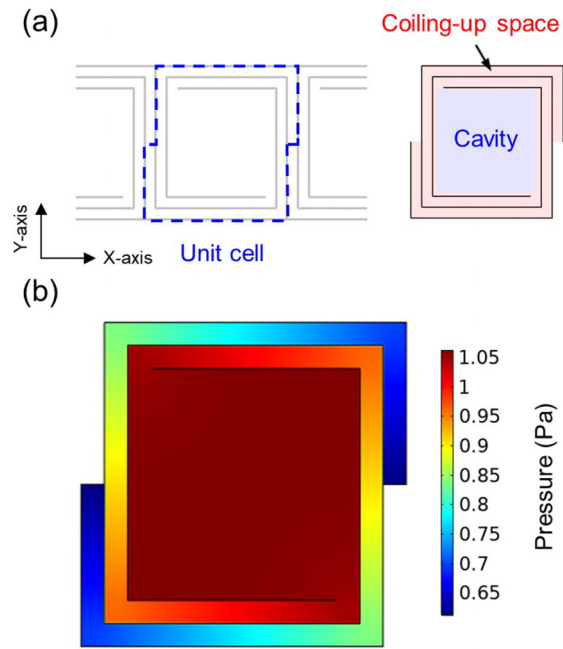

FIG. 2. (a) Unit cell of metamaterial and design concept of unit cell; (b) mode shape of unit cell.

In addition to the coiling-up space that amplifies the nonlinear effect, we used the concept of the Bragg gap to suppress the generation of undesired frequencies. To utilize the Bragg gap phenomenon, an acoustic cavity was placed inside the mazelike structure. Owing to the acoustic cavity, a standing wave was formed at a certain frequency from which a Bragg gap was formed. Hence, the generation of undesired frequencies can be suppressed by adjusting the geometry of the cavity to generate the Bragg gap, which includes the undesired frequencies. It is noteworthy that the band gap can also be achieved based on other physics such as internal resonance. However, the Bragg gap was considered in this study because the frequency conversion involved multiple frequencies, and hence a broad stop band was required.

Figure 2 shows the final metamaterial design based on the investigations above. As shown, our metamaterial comprised an acoustic cavity surrounded by a mazelike structure. Here, the mazelike structure provides an extremely low wave speed, whereas the cavity provides a Bragg gap that suppresses undesired frequencies. In addition, the number of unit cells is properly chosen to enhance the frequency conversion, which will be explained later. Hence, the acoustic frequency conversion can be improved significantly.

In the above explanations, the design approach is roughly introduced with the well-known physics of linear metamaterials. However, because the main topic, frequency down-conversion, is a nonlinear phenomenon, the detailed physics of the proposed metamaterial should be studied first. In particular, we would like to focus on the increased density effect, and the multifrequency Fabry-Perot resonance effect, which cannot be found in linear cases.

A. Effect of coiling-up space on frequency conversion

To investigate the physics of the frequency conversion inside the coiling-up space, we consider the following frequency
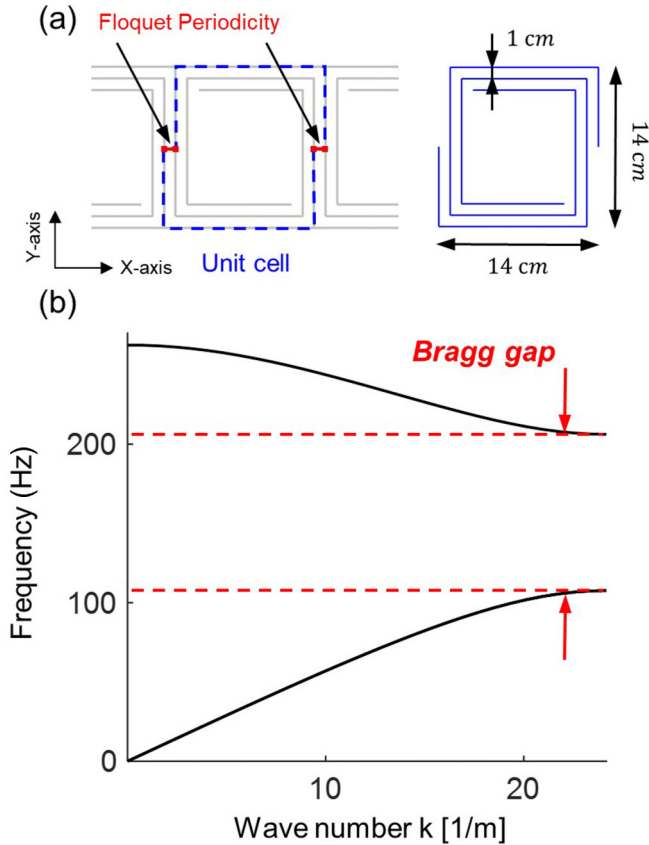
FIG. 3. (a) Boundary conditions for eigenfrequency analysis and size of unit cell; (b) the numerically calculated wave dispersion curve.

FIG. 4. (a) Effective sound speed; (b) effective density of metamaterial calculated by transfer matrix method.

down-conversion example. Based on the incident acoustic wave of the frequency $f_1 = 100$ Hz, our goal is to add modulating acoustic waves of the frequency $f_2 = 70$, 80, and 90 Hz to achieve frequency down-conversions of 30, 20, and 10 Hz, respectively. As a nonlinear medium, air with density $\rho = 1.204$ kg/m^3, speed of sound $c = 343$ m/s, and nonlinear coefficient $\beta = 1.2$ was considered [4]. It is noteworthy that in a nonlinear system, the effective properties change as the wave's amplitude changes [32–34]. However, if the amplitude is sufficiently small, the effective properties are almost the same as in the linear case, regardless of the amplitude. Here, we used the amplitude of 5 kPa, which is sufficiently small so that the effective parameters are almost the same as the linear case and almost unaltered as the amplitude changes. The dispersion curve of the metamaterial, calculated by considering the nonlinear effect, is shown in Fig. 3(b). It is clear that the proposed metamaterial has a band gap from 107 to 206 Hz, which can effectively suppress the undesired frequencies generated during the frequency conversion.

Based on the metamaterial design, the metamaterial's effective properties were calculated by considering the nonlinear effect to investigate the physics associated with frequency conversion in the coiling-up space. The metamaterial's effective properties, including its extremely low effective wave speed by the mazelike structure, were verified using the transfer matrix method (see the detailed process in Appendix A)
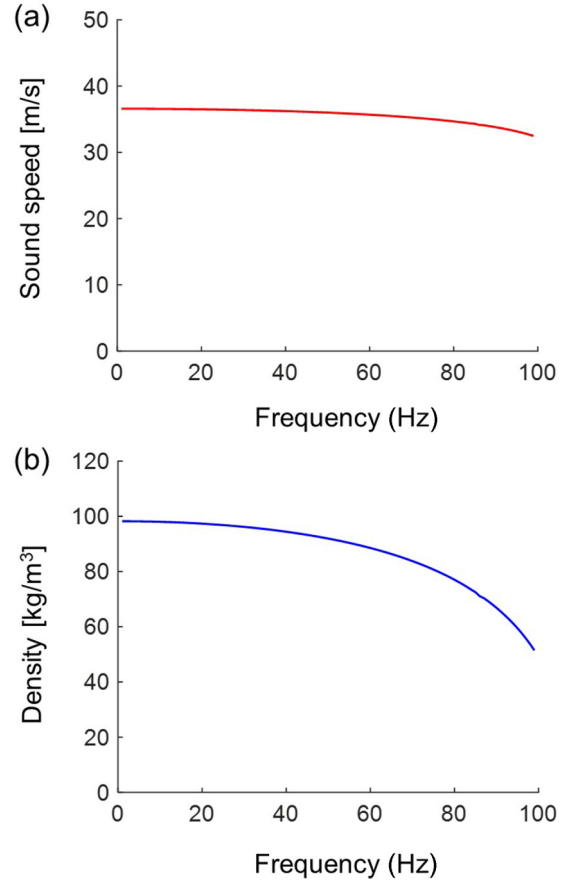
[35,36]. The proposed acoustic metamaterial's effective sound speed and effective density, calculated using the transfer matrix method, are shown in Fig. 4. An analysis of the calculated results shows that the effective sound speed decreased significantly compared with the original sound speed (343 m/s), as shown in Fig. 4(a), which has been reported previously. By contrast, the effective density of the metamaterial increased significantly, as shown in Fig. 4(b). The effective density was approximately 100 kg/m^3, whereas the original air density was 1.024 kg/m^3.

This suggests that, unlike our initial expectation, the coiling-up space does not always enhance the frequency conversion. One may assume that the coiling-up space causes the wave to remain longer inside, thereby enhancing the nonlinear effect. However, as shown in Fig. 4(b), the coiling-up space not only exhibits a low wave speed, but also an increased density effect. As shown in Eq. (14), the increased density effect adversely affected the frequency conversion. Hence, the performance of the coiling-up space metamaterial for frequency conversion was worse than expected. This will be demonstrated based on numerical simulation results in the next section. In addition, this finding suggests that the frequency conversion effect can be further enhanced if a method that can reduce the effective density of the coiling-up space is available.

Nevertheless, the resulting frequency conversion is expected to improve when using the designed metamaterial.

Because the amplitude of the converted frequency is inversely proportional to the density, an increase in the effective density decreases the amplitude of the frequency down-converted wave. However, because the amplitude of the converted frequency is inversely proportional to the cube of the wave speed, the decrease in the wave speed can significantly increase the frequency conversion. In addition, because the effective material properties are applicable for broad frequencies, the proposed metamaterial is suitable for enhancing the frequency down-conversion, which involves multiple frequencies.

B. Effect of multifrequency Fabry-Perot resonance of metamaterial system

In general, it is almost impossible to avoid the Fabry-Perot resonance in metamaterial structures. In previous linear metamaterials, only a single frequency has been considered in the Fabry-Perot resonance. However, in the current research, various frequency components are involved so that multifrequency Fabry-Perot resonance should be considered.

First, it is obvious that the Fabry-Perot resonance at the incident frequencies, ω_1 and ω_2, affects the frequency conversion—although the incident waves are actuated with the amplitudes of A_1 and A_2, their amplitudes can be changed due to the Fabry-Perot resonance inside the metamaterial so that the overall frequency conversion can be altered.

In addition to the incident frequencies, the Fabry-Perot resonance at the frequency-converted wave, $|\omega_1 - \omega_2|$, also affects the frequency conversion. To explain this, let us revisit Eq. (2), the Westervelt equation again. Comparing Eq. (2) with the linear acoustic equation, it can be seen that the nonlinear equation can be considered as the linear acoustic equation with distributed nonlinear monopole source. In other words, the frequency conversion can be seen as the linear wave propagation with distributed nonlinear monopole source having the frequency of $|\omega_1 - \omega_2|$. Considering that wave generated by the distributed wave source is largely enhanced by the Fabry-Perot resonance, it can be concluded that the Fabry-Perot resonance at the frequency-converted wave also affects the frequency conversion. In summary, the amount of the frequency-converted wave from the acoustic metamaterial can be predicted as

$$\frac{\beta A_1 A_2 (\omega_1 - \omega_2) l}{2 \rho_0 c_0^3} W_1 W_2 W_3. \tag{15}$$

where W_1, W_2, and W_3 are the transmission ratio calculated from the Fabry-Perot resonance at the frequencies of ω_1, ω_2 and $|\omega_1 - \omega_2|$ respectively. Also, l is the metamaterial's length.

In the metamaterial design, the number of the metamaterial's unit cell, 10 unit cells, is properly chosen with the Fabry-Perot resonance effect. Considering that the Fabry-Perot resonance takes place when the metamaterial length becomes $n\lambda/2$ (n is an integer) [37], it is convenient to use the supercell approach with the whole metamaterial system in the simulation, 10 unit cells, as a unit cell. With this supercell approach, the frequencies where the Fabry-Perot resonance takes place become the same as the frequencies corresponding to the Γ and χ points, as shown in Fig. 5(a). Accordingly, the metamaterial is designed to have the Fabry-
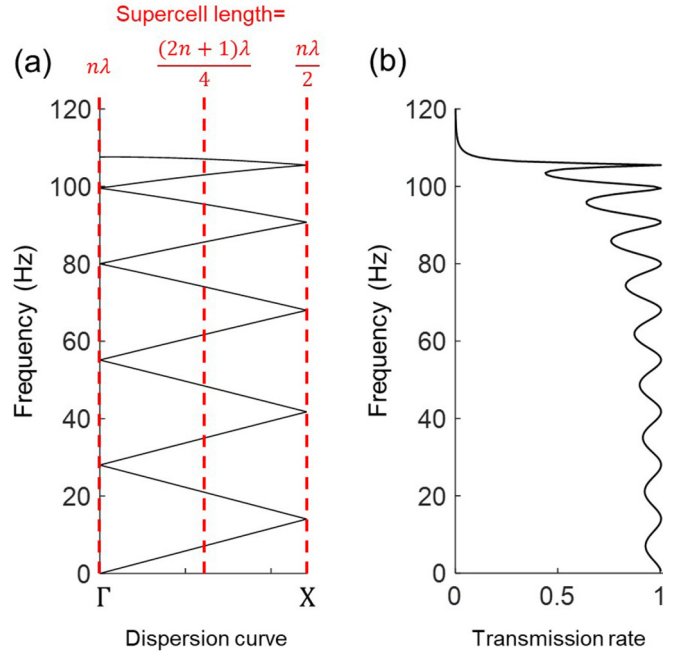

FIG. 5. (a) Dispersion curve calculated by considering the entire metamaterial as one supercell and (b) transmission rate according to frequency.

Perot resonance at the considered incident frequencies, 100, 90, 80, and 70 Hz. The effect of the Fabry-Perot resonance can be clearly seen from Fig. 5(b), which plots the wave transmission ratio, i.e., the ratio of the transmitted wave's amplitude and the incident wave's amplitude. It is noteworthy that it would be best to additionally consider the Fabry-Perot resonance at the frequency-converted waves, $|\omega_1 - \omega_2|$, in the metamaterial design. However, as can be seen in Fig. 5(b), the effect of the Fabry-Perot resonance is not very significant at low-frequency ranges so that we only considered the incident waves in the design. Nevertheless, in predicting the amount of the frequency-converted waves, the Fabry-Perot resonance at the frequency-converted waves is also considered as in Eq. (15).

C. Numerical validation of the acoustic metamaterial

Using the numerical method, the performance of the metamaterial was validated by comparing the numerical results of the normal duct with the results of the metamaterial. The numerical simulation models of the normal duct and metamaterial are shown in Fig. 6. As shown in Fig. 6(b), the metamaterial simulation model comprised 10 unit cells.

Numerical simulations of the normal duct and metamaterial were performed under the same conditions. In both cases, a pressure wave was actuated at the left end and the radiation condition was applied to the right end. The transmitted wave was measured at the right end, where the radiation condition was applied. Because our focus was on the acoustic frequency conversion, both the incident and modulating waves were actuated simultaneously. Based on the boundary and actuating conditions, a time-transient wave simulation was performed. Inside the duct and metamaterial, nonlinear acoustic air with
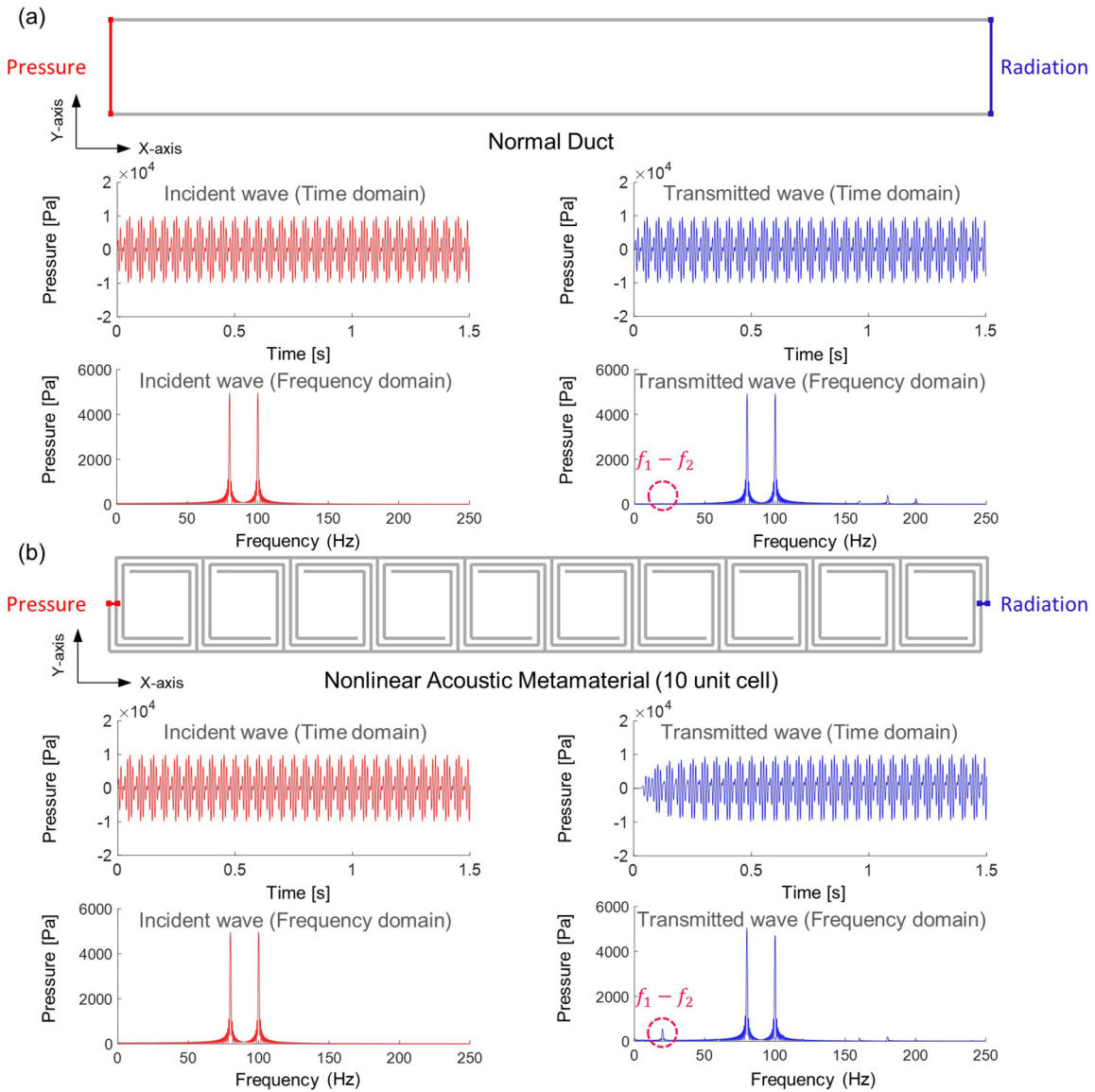
FIG. 6. The numerical simulation model, boundary conditions, and simulation results of incident wave and transmitted wave where $f_1 = 100$ Hz, $f_2 = 80$ Hz for (a) normal duct, and (b) metamaterial.

density $\rho = 1.024$ kg/m^3, speed of sound $c = 343$ m/s, and nonlinear coefficient $\beta = 1.2$ was considered. The numerical simulations were performed for three cases, where the frequency of the incident wave (f_1) was 100 Hz and the frequencies of the modulating wave (f_2) were 90, 80, and 70 Hz.

The time-domain raw data measured at both ends of the normal duct and metamaterial were converted into the frequency domain by fast Fourier transform (FFT). The time- and frequency-domain data, measured in a simulation where f_1 was 100 Hz and f_2 was 80 Hz, are shown in Figs. 6(a) and 6(b), respectively. The sampling time was set to 1.5 s. As shown in Fig. 6, the time required for the wave to reach the right end of the normal duct was much shorter than that required for the metamaterial case. This means that the metamaterial had an extremely low wave speed, as desired. Analyzing the frequency domain data, we observed the effect of the low effective sound speed on the amplitude of the

frequency down-converted wave. Comparing the transmitted wave data of the normal duct and metamaterial in the frequency domain, we verified that the amplitude of 20 Hz, corresponding to the frequency down-converted wave, was significantly amplified in the metamaterial case.

The overall results of the numerical simulations are shown in Fig. 7. The results shown in Figs. 7(a)–7(c) are the frequency-domain data of the transmitted wave when the frequency of the incident wave (f_1) is 100 Hz and the frequencies of the modulating wave (f_2) are 90, 80, and 70 Hz, respectively. As shown in Fig. 7, the frequency down-converted wave of the normal duct is too small to be distinguished from the ambient noise, whereas the frequency down-converted wave of the metamaterial is clearly distinguishable. In other words, the amplitudes of 10, 20, and 30 Hz, which correspond to the frequency down-converted wave of each simulation, were amplified significantly in the metamaterial. It is noteworthy that in Fig. 7, the amplitudes of the frequency
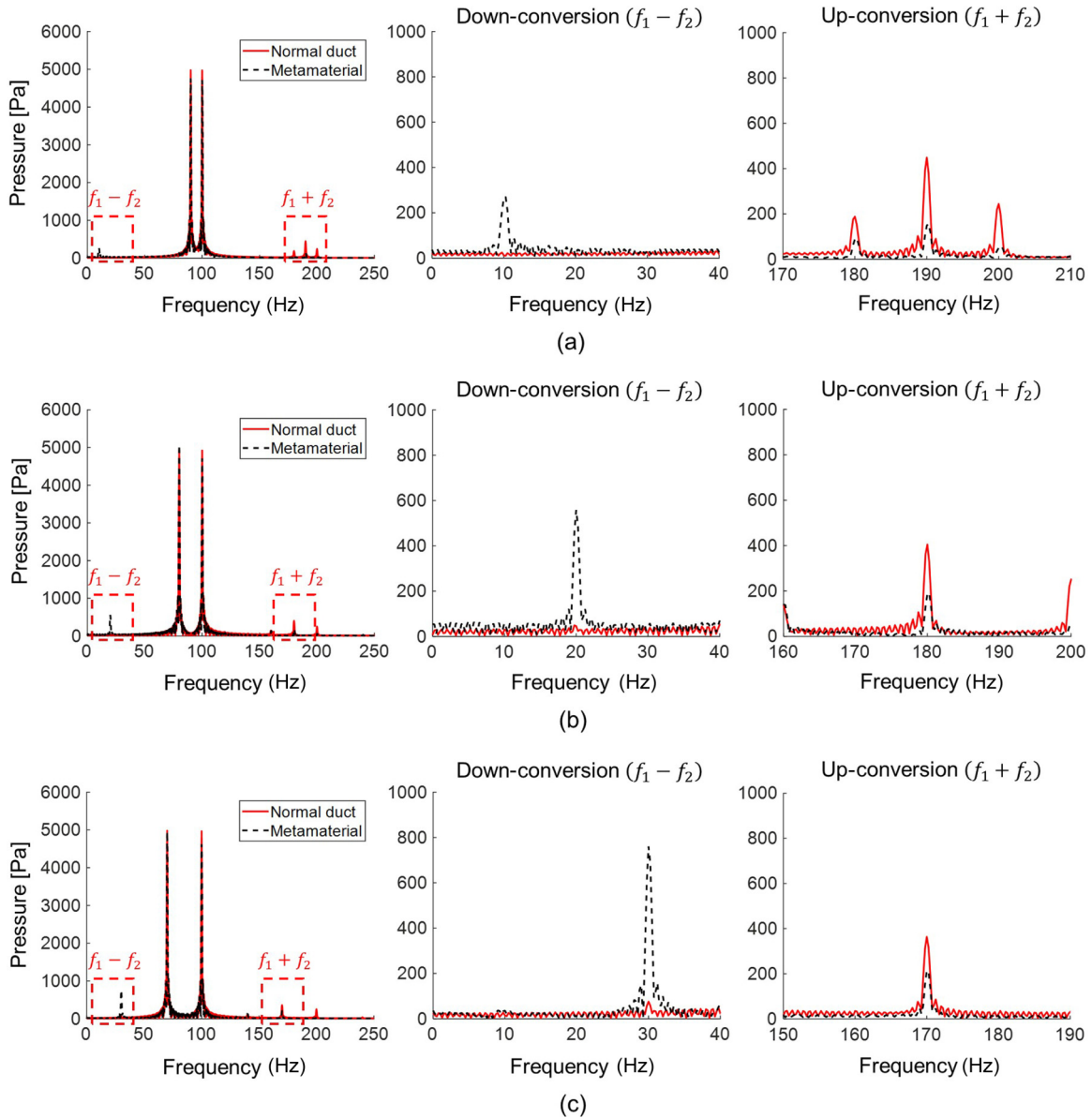
FIG. 7. The numerical simulation results of transmitted waves in normal duct and metamaterial for $f_1 = 100$ Hz and $f_2 =$ (a) 90, (b) 80, and (c) 70 Hz.

down-converted waves increased with the frequency. This is because the amplitude of the converted frequency is proportional to the converted frequency in the acoustic frequency conversion, as shown in the second perturbation solution of the background theory, Eq. (14).

As shown in the high-frequency region in Fig. 7, the amplitudes of the undesired frequency components, i.e., the frequency up-converted wave and the second-harmonic wave, decreased in the metamaterial rather than in the normal duct. According to theory, the amplitudes of the frequency up-converted wave and the second-harmonic wave must increase as the effective speed of sound decreases. However, as shown in Fig. 7, they were suppressed by the Bragg gap. In conclusion, the numerical results show that the efficiency of the frequency down-conversion improved by the acoustic metamaterial, which amplified the frequency down-converted wave and suppressed undesired waves such as the second harmon-

ics and the frequency up-converted wave, which may cause undesired intermodulation.

Based on the results, we verified the physics of the metamaterial. In the normal duct case, the analytically calculated amplitudes of the frequency down-conversion agreed well with the numerical results in the normal duct (the analytical results for 10, 20, and 30 Hz were 25.2, 51.84, and 75.68 Pa, whereas the numerical results were 25.218, 50.435, and 75.653 Pa). On the other hand, in the metamaterial case, the numerically measured amplitudes of the frequency down-conversion were 264.8, 558.4, and 760.7 Pa for 10, 20, and 30 Hz, respectively. If we ignore the two major effects, "the increased density effect" and "the multifrequency Fabry-Perot resonance effect," the analytically predicted amplitudes of the frequency down-conversion are calculated as 25 645.3, 51 290.5, and 76 935.8 Pa for 10, 20, and 30 Hz cases, respectively, which are largely different from the numerically
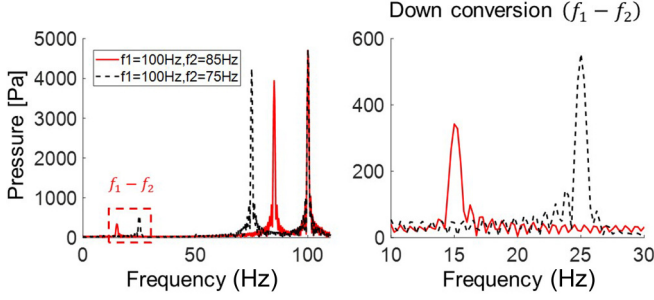
FIG. 8. The numerical simulation results of transmitted waves in metamaterial for $f_1 = 100$ Hz and $f_2 = 85, 75$ Hz.

measured values. On the other hand, if two effects are considered as in Eq. (15), the analytically predicted amplitudes will be 258.048, 515.121, and 785.294 Pa for the 10, 20, and 30 Hz cases, respectively, which are much closer to the numerically calculated results. This strongly validates that both the increased density effect and the multifrequency Fabry-Perot resonance effect are important in the frequency conversion with nonlinear metamaterials.

To further support the multifrequency Fabry-Perot resonance effect, additional simulations are performed for two cases—the first case has the incident waves at 100 and 85 Hz, and the second case, at 100 and 75 Hz. It is noteworthy that both 100 Hz is near to the Fabry-Perot resonance frequency while 85 and 75 Hz are near to the Fabry-Perot antiresonance frequencies when the transmission rates are 0.7709 and 0.8348. From the results plotted in Fig. 8, it can be clearly seen that the Fabry-Perot resonance significantly affects the frequency down-conversion—it can be seen that the incident waves of the Fabry-Perot antiresonance frequencies (75 and 85 Hz, respectively) are largely decreased compared to the incident wave of the Fabry-Perot resonance frequency (100 Hz). Obviously, the decrease adversely affects the frequency-converted waves corresponding to $|\omega_1 - \omega_2|$ so that their amplitudes are decreased. If the effect of the Fabry-Perot resonance is ignored as in Eq. (14), the analytical calculation yields the amount of the frequency conversion as 428.397 and 713.995 Pa, which are largely different from the numerically calculated results of 342.2 and 553.7 Pa. However, if the Fabry-Perot resonance is considered as in Eq. (15), the analytic prediction will be 319.452 and 558.852 Pa, which agree well with the numerical results.

Table I shows the analytically predicted and numerically calculated frequency-converted waves for various cases con-

sidered in this work. As shown in Table I, Eq. (15) can well predict the frequency-converted wave, validating the increased density effect and the multifrequency Fabry-Perot resonance effect reported here.

IV. EFFECT OF DISSIPATION

In metamaterials, the dissipation effect cannot be neglected, particularly when a coiling-up space is applied, as in current acoustic metamaterials [38]. Moreover, because the nonlinear effect is involved in the current metamaterial, one may argue that the effect of dissipation may alter the nonlinear effect, causing other undesired nonlinear phenomena to occur. Therefore, wave dissipation in nonlinear acoustic metamaterials will be analytically and numerically investigated herein.

First, the effect of wave dissipation in nonlinear acoustics is analytically investigated to determine whether the dissipation may generate other undesired nonlinear phenomena. Sound dissipation is caused by various loss mechanisms such as viscosity, heat conduction, and boundary layer effects. Among them, assuming an adiabatic process, dissipations due to viscosity and boundary layer effects are generally considered as dominant factors, whereas other loss mechanisms are typically neglected. In this section, both loss mechanisms and nonlinear effects are considered to determine how the dissipation effects alter the nonlinear effects. Following the procedures provided in Appendix B, the nonlinear acoustic equation, including both viscosity and nonlinearity, is expressed as

$$\Delta p - \frac{1}{c_0^2}\frac{\partial^2 p}{\partial t^2} = -\frac{\beta}{\rho_0 c_0^4}\frac{\partial^2 p^2}{\partial t^2} - \frac{1}{\rho_0 c_0^2}\left(\frac{4}{3}\mu + \mu_B\right)\Delta\frac{\partial p}{\partial t}. \quad (16)$$

In Eq. (15), p, c_0, β, μ, and μ_B denote the pressure, wave speed, nonlinearity coefficient, shear viscosity coefficient, and bulk viscosity coefficient, respectively. Comparing Eq. (16) with the lossless nonlinear acoustic equation in Eq. (2), it is clear that the only difference in the lossy nonlinear equation in Eq. (16) is the addition of the lossy term, $\Delta(\partial p_d/\partial t)$. In other words, the loss effect does not affect the nonlinear term, $\partial^2 p_d^2/\partial t^2$. Hence, it is clear that the dissipation does not alter the nonlinear effect and does not provide any undesired nonlinear phenomena.

However, owing to the effect of dissipation, the amplitudes for each frequency wave decayed as they propagated. Considering that the high-frequency waves are more vulnerable to the

TABLE I. The analytically predicted and numerically calculated amplitudes of frequency down-converted waves.

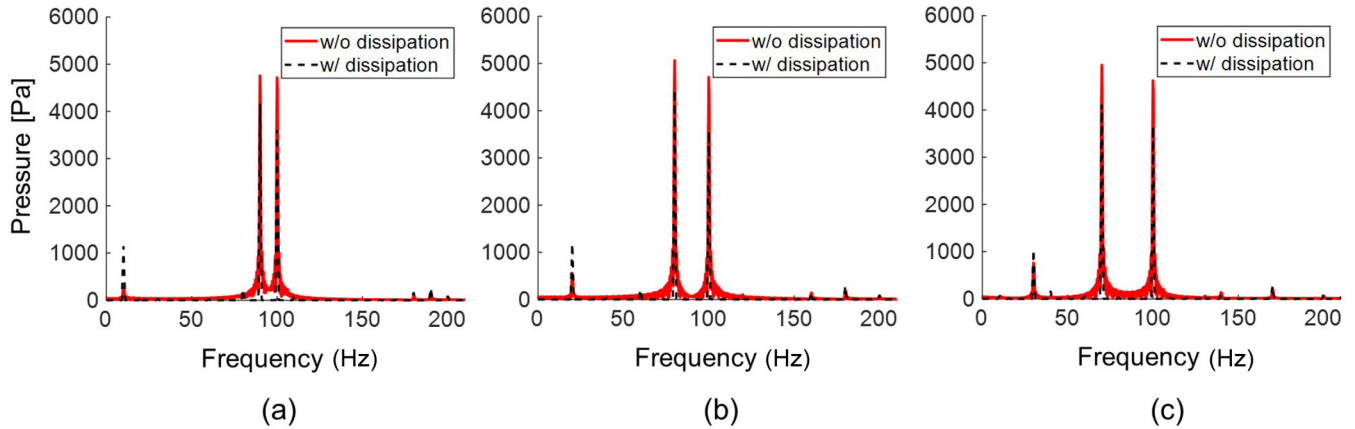| Freq ($f_1 - f_2$)	Transmission rate (Fabry-Perot resonance)			Amplitude	
	W_1	W_2	W_3	Analytical	Numerical
10 Hz	0.9673	0.9784	0.9547	258.048 Pa	264.8 Pa
15 Hz	0.9673	0.7709	1	319.452 Pa	342.2 Pa
20 Hz	0.9673	1	0.9286	515.121 Pa	558.4 Pa
25 Hz	0.9673	0.8348	0.9693	558.852 Pa	553.7 Pa
30 Hz	0.9673	0.9605	0.9865	785.294 Pa	760.7 Pa

FIG. 9. The numerical simulation results of transmitted waves in metamaterial without and with dissipation for $f_1 = 100$ Hz and $f_2 =$ (a) 90, (b) 80, and (c) 70 Hz.

dissipation effect, the frequency down-converted wave having the lowest frequency will be the least affected wave; i.e., the relative amount of the frequency down-converted wave will increase owing to the dissipation. Consequently, one can expect that the dissipation effect will not degrade the frequency down-conversion; moreover, the dissipation will be beneficial because other waves are effectively dissipated.

Next, we discuss the wave simulation. It might be ideal to perform experiments; however, owing to the lack of available actuators that can actuate sufficiently large amplitudes with two different frequencies simultaneously, we performed numerical simulations instead, using COMSOL MULTIPHYSICS, a commercial finite element method (FEM) program. To consider the viscosity and nonlinearity, as in Eq. (16), the linearized Navier-Stokes module was used with a domain source, where $\mu = 1.846 \times 10^{-5}$ [kg m^{-1} s^{-1}] and $\mu_B = 1.5 \times 10^{-5}$ [kg m^{-1} s^{-1}] were used as the shear and bulk viscosity coefficients of air at room temperature, respectively [39]. Dissipation due to boundary layer effects was also considered by applying the no-slip condition to the wall. The other settings, except the dissipation, were the same as in the previous simulation. The numerical simulation results considering dissipation are shown in Fig. 9. The results shown in Fig. 9, which were obtained by the FFT of the measured data, are plotted in the frequency domain. Here, the frequency of the incident wave (f_1) was 100 Hz, and the frequencies of the modulating wave (f_2) were 90, 80, and 70 Hz, respectively. As shown in Fig. 9, the amplitudes of the incident waves (f_1) and modulating waves (f_2) corresponding to the fundamental waves attenuated significantly owing to dissipation. In addition, the frequency up-converted waves ($f_1 + f_2$) and second-harmonic waves ($2f_1, 2f_2$) almost dissipated. By contrast, the amplitudes of the frequency down-converted waves ($|f_1 - f_2|$) were not significantly attenuated. This is due to the characteristics of dissipation and frequency conversion. According to theory, dissipation by viscosity is proportional to the square of the frequency, and that dissipation by boundary layer effects is proportional to the square root of the frequency. Therefore, attenuation by dissipation is insignificant for the frequency down-converted wave, as explained earlier.

It is interesting that the frequency-converted waves have larger amplitudes for lossy cases, as shown in Fig. 9. This

is because the acoustic wave speed is decreased by the no-slip condition. In the proposed metamaterial, the acoustic wave propagating inside the metamaterial can be considered as the acoustic waves inside a duct. Inside the duct, fluid particles adjacent to the wall do not oscillate because of the no-slip condition. If the fluids are inviscid, then the particle can slip over the wall, and boundary layer effects can be neglected [40]. However, for viscous fluids in which viscosity loss is considered, the particle oscillation decreases from its amplitude in the mainstream to zero at the wall (this effect is known as the boundary layer effect). Consequently, the wave inside the metamaterial is decelerated (this can be verified by numerical simulations, where the wave's arrival time is delayed for the lossy case). Accordingly, the frequency down-conversion occurs more frequently. Consequently, the frequency down-conversion is significantly enhanced owing to the no-slip condition, as shown in Fig. 9. It is noteworthy that other types of damping, such as the viscous effect, do not enhance the frequency conversion because they do not decelerate the wave speed.

Based on the numerical simulation results, it was verified that the dissipation effect was insignificant, and that the frequency down-converted waves were not dissipated significantly. In addition, the dissipation effect did not adversely affect the frequency down-conversion. The performance of the proposed metamaterial was valid even when dissipation was considered. In this study, the frequency down-conversion was considered such that the cavity had a band gap encompassing $f_1 + f_2$; however, the same idea is applicable to the frequency up-conversion case by designing the band gap to encompass the frequency of $|f_1 - f_2|$.

V. CONCLUSIONS

Herein, we proposed an acoustic metamaterial for efficient frequency down-conversions. Based on the second perturbation solution obtained from the Westervelt equation, we discovered that the amplitude of the frequency down-converted wave was inversely proportional to the cube of the speed of sound. In addition, we discovered that the undesired intermodulation generated from frequency up-converted waves and harmonics can serve as noise. To achieve both
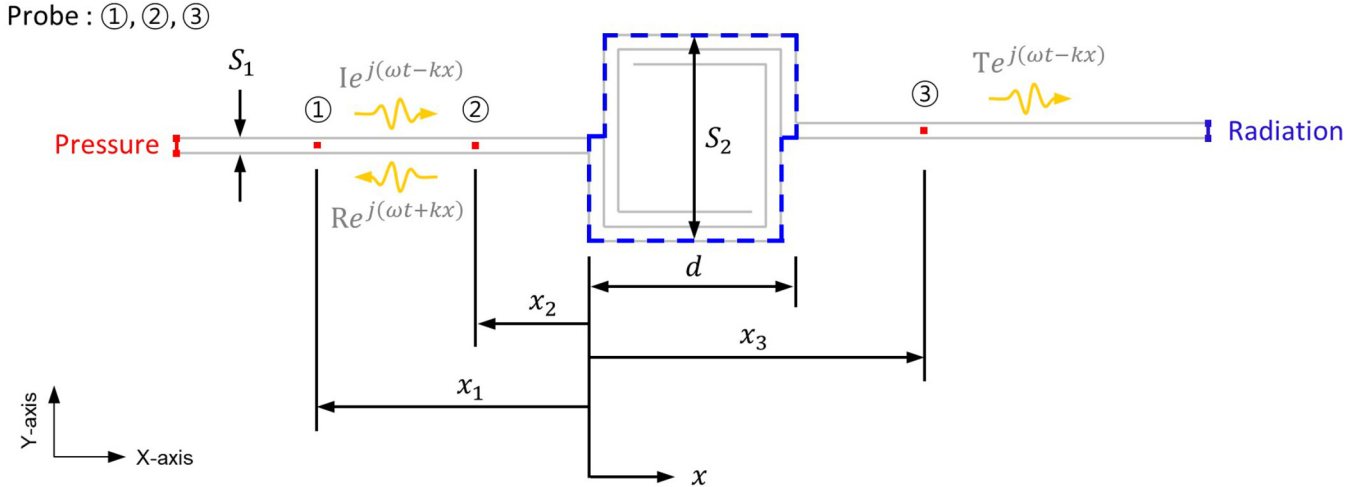
FIG. 10. Numerical simulation model for transfer matrix method to obtain effective properties of metamaterial.

the amplification of the frequency down-converted wave and the suppression of undesired intermodulation, we developed an acoustic metamaterial based on the coiling-up space and Bragg gap. The Bragg gap suppresses the undesired intermodulation by preventing the propagation of the frequency up-converted waves and harmonics, whereas the coiling-up space amplifies the amplitude of the frequency down-converted waves by decreasing the effective speed of sound. Furthermore, we found the increased density effect and the multifrequency Fabry-Perot resonance effect in the nonlinear frequency conversion of the acoustic metamaterial. Numerical and analytical investigations demonstrated that the efficiency of the frequency down-conversion improved when the proposed metamaterial was used. In addition, further investigation showed that dissipation did not adversely affect the performance of the proposed metamaterial. Considering that frequency conversion is affected by the small amplitude of the converted frequency and undesired intermodulation, the results presented herein would be useful for frequency conversion in acoustics.

APPENDIX A: TRANSFER MATRIX METHOD

The transfer matrix method is used to calculate the effective properties of the nonlinear acoustic metamaterial [35]. The measurement values required for the transfer matrix method are obtained by the time-harmonic numerical simulation. The numerical simulation model is shown in Fig. 10. As shown in Fig. 10, the numerical simulation model consists of additional ducts and the unit cell of the proposed acous-

tic metamaterial. In the case of the boundary conditions, a pressure wave is actuated at the left end of the model and the radiation condition is applied at the other end to prevent a reflected wave. To measure the pressures required for the transfer matrix method, three measurement points located at x_1, x_2, and x_3 respectively, are set in the additional duct section. The pressures measured at each measurement point are denoted as P_1, P_2, and P_3 in Fig. 10. The measured pressures are the superpositions of incident and reflected plane waves, so that complex pressures, P_1, P_2, and P_3, can be expressed in terms of the coefficients I, R, and T as

$$P_1 = (Ie^{-jkx_1} + Re^{jkx_1})e^{j\omega t}, \tag{A1}$$

$$P_2 = (Ie^{-jkx_2} + Re^{jkx_2})e^{j\omega t}, \tag{A2}$$

$$P_3 = (Te^{-jkx_3})e^{j\omega t}, \tag{A3}$$

where k represents the wave number. Rewriting Eqs. (A1)–(A3) with respect to the coefficients I, R, and T yields

$$I = \frac{j(P_1 e^{jkx_2} - P_2 e^{jkx_1})}{2\sin k(x_1 - x_2)}, \tag{A4}$$

$$R = \frac{j(P_2 e^{-jkx_1} - P_1 e^{-jkx_2})}{2\sin k(x_1 - x_2)}, \tag{A5}$$

$$T = P_3 e^{jkx_3}. \tag{A6}$$

Now, consider the transfer matrix which relates the sound pressures and normal acoustic particle velocities on the left and right surfaces of the metamaterial shown in Fig. 10. The transfer matrix is expressed as

$$\begin{bmatrix} P_L \\ V_L \end{bmatrix} = \begin{bmatrix} T_{11} & T_{12} \\ T_{21} & T_{22} \end{bmatrix} \begin{bmatrix} P_R \\ V_R \end{bmatrix}, \tag{A7}$$

where P is the exterior sound pressure and V is the exterior normal acoustic particle velocity. Also, the subscripts R and L indicate that the variable is measured at the right and left surface of the metamaterial, respectively. Considering the cross-sectional area of duct S_1 as shown in Fig. 10, the

pressures and the particle velocities on the two surfaces of the metamaterial are expressed in terms of the coefficients I, R, and T as

$$P_L = I + R, \tag{A8}$$

$$V_L = S_1 \frac{I - R}{\rho_0 c}, \tag{A9}$$

$$P_R = T e^{-jkd}, \tag{A10}$$

$$V_R = S_1 \frac{T e^{-jkd}}{\rho_0 c}, \tag{A11}$$

where ρ_0 is the fluid density, c is the sound speed, and S_1 is the cross-section area of the extended duct. Thus, when the coefficients I, R, and T for the incident, reflected, and transmitted waves are known, the pressures and the particle velocities on the two surfaces of the metamaterial can be determined. However, Eq. (A7) and Eqs. (A8)–(A11) are not enough to retrieve the transfer matrix since only two equations can be obtained while four unknowns, T_{11}, T_{12}, T_{21}, and T_{22}, should be calculated. Thus, two additional equations are required to solve the transfer matrix elements. Those equations can be obtained by using reciprocal nature. The reciprocity requires that the determinant of the transfer matrix should be unity [35,36]. Additionally, for symmetrical systems, T_{11} is equal to T_{22}. Thus, two more equations are given as

$$T_{11} = T_{22}, \tag{A12}$$

$$T_{11}T_{22} - T_{12}T_{21} = 1. \tag{A13}$$

By combining Eq. (A7) and Eqs. (A12) and (A13), the transfer matrix elements can be derived in terms of the pressures and the particle velocities on the two surfaces of the metamaterial as

$$T_{11} = \frac{P_R V_R + P_L V_L}{P_L V_R + P_R V_L}, \tag{A14}$$

$$T_{12} = \frac{P_L^2 - P_R^2}{P_L V_R + P_R V_L}, \tag{A15}$$

$$T_{21} = \frac{V_L^2 - V_R^2}{P_L V_R + P_R V_L}, \tag{A16}$$

$$T_{22} = \frac{P_R V_R + P_L V_L}{P_L V_R + P_R V_L}. \tag{A17}$$

As transfer matrix elements are known, effective properties of the metamaterial can be calculated. From the classical acoustics, the acoustic media with the thickness d and cross-sectional area of S_2 are given as

$$\begin{bmatrix} T_{11} & T_{12} \\ T_{21} & T_{22} \end{bmatrix} = \begin{bmatrix} \cos k_e d & j\rho_e c_e \sin k_e d / S_2 \\ jS_2 \sin k_e d / \rho_e c_e & \cos k_e d \end{bmatrix}, \tag{A18}$$

where k_e is the wave number and $\rho_e c_e$ is the characteristic impedance of the acoustic media. Therefore, the wave number and characteristic impedance can be calculated from the components of the transfer matrix as

$$k_e = \frac{1}{d}\cos^{-1} T_{11}, \tag{A19}$$

or

$$k_e = \frac{1}{d}\sin^{-1}\sqrt{-T_{12}T_{21}}, \tag{A20}$$

$$\rho_e c_e = \sqrt{T_{12}/T_{21}}. \tag{A21}$$

As k_e and $\rho_e c_e$ are determined, effective properties of the metamaterial, such as effective sound speed and effective density, can be easily calculated as

$$c_e = \omega d / \sin^{-1}\sqrt{-T_{12}/T_{21}}, \tag{A22}$$

$$\rho_e = \sqrt{T_{12}/T_{21}}/c_e. \tag{A23}$$

APPENDIX B: THEORETICAL INVESTIGATION OF DISSIPATION WITH NONLINEARITY

Sound dissipation is caused by various loss mechanisms such as viscosity, heat conduction, boundary layer effects, etc. Among them, assuming an adiabatic process, dissipations due to viscosity and boundary layer effects are generally considered as dominant factors while other loss mechanisms are usually neglected. In this section, an acoustic wave equation will be derived with both loss mechanisms and nonlinear effects to figure out how the dissipation effects change the nonlinear effects. To this end, three equations—continuity, state, and momentum equations–are required. Before deriving detailed equations, acoustic variables such as pressure, density, and velocity are expressed with the time-averaged terms and dynamic fluctuating terms as

$$p = p_0 + p_d, \tag{B1}$$

$$\rho = \rho_0 + \rho_d, \tag{B2}$$

$$\mathbf{u} = \mathbf{u}_0 + \mathbf{u}_d, \tag{B3}$$

where subscript 0 and d indicate time-averaged term and dynamic fluctuating term, respectively. Generally, the time-averaged velocity is set to be zero as $\mathbf{u}_0 = 0$ so that

$$\mathbf{u} = \mathbf{u}_d. \tag{B4}$$

Based on Eqs. (B1)–(B3), the continuity equation is considered first. Considering the nature of continuity, it is obvious that the continuity equation does not change whether the system is nonlinear or lossy. Therefore, the well-known acoustic continuity equation is used here as

$$\frac{\partial \rho_d}{\partial t} + \rho_0 \nabla \cdot \mathbf{u}_d = \frac{p_d}{\rho_0 c_0^4}\frac{\partial p_d}{\partial t} - \frac{1}{c_0^2}\mathbf{u}_d \cdot \nabla p_d. \tag{B5}$$

In the same manner, the state equation, which relates pressure and density, is affected by the acoustic media's material property. Thus, the equation is largely affected by the nonlinear effect. According to the Westervelt equation, the state equation for nonlinear media is given as [25]

$$\rho_d \cong \frac{p_d}{c_0^2}\left[1 - (\beta - 1)\frac{p_d}{\rho_0 c_0^2}\right]. \tag{B6}$$

As can be seen in Eq. (B6), the effect of nonlinearity is considered in the state equation, but the loss effect has nothing to do with it. This is quite obvious since the loss is not related to the density-pressure relationships—it only dissipates energy and decreases the amplitude.

On the other hand, the momentum equation, which is closely related to the energy, is dominated by the loss effect rather than the nonlinear effect. The momentum equation for lossy acoustic media is given as [40]

$$\rho \frac{D\mathbf{u}}{Dt} + \nabla p = \left(\frac{4}{3}\mu + \mu_B\right)\nabla(\nabla \cdot \mathbf{u}) - \mu\nabla \times \nabla \times \mathbf{u}, \quad (B7)$$

where μ and μ_B denote shear viscosity coefficient and bulk viscosity coefficient. Here, the material derivative is defined as

$$\frac{D}{Dt} = \frac{\partial}{\partial t} + \mathbf{u} \cdot \nabla. \quad (B8)$$

With Eq. (B8), Eq. (B7) can be rewritten as

$$(\rho_0 + \rho_d)\left[\frac{\partial \mathbf{u}_d}{\partial t} + (\mathbf{u}_d \cdot \nabla)\mathbf{u}_d\right] + \nabla(p_0 + p_d)$$

$$= \left(\frac{4}{3}\mu + \mu_B\right)\nabla(\nabla \cdot \mathbf{u}_d) - \mu\nabla \times \nabla \times \mathbf{u}_d. \quad (B9)$$

Equation (B9) can be more simplified by using the plane wave relationship as [41]

$$\rho_d \frac{\partial \mathbf{u}_d}{\partial t} = -\nabla\left(\frac{p_d^2}{2\rho_0 c_0^2}\right), \quad (B10)$$

and the identities of $(\mathbf{u}_d \cdot \nabla)\mathbf{u}_d = \nabla(\mathbf{u}_d^2/2)$ and $\nabla \times \nabla \times \mathbf{u} = \nabla(\nabla \cdot \mathbf{u}) - \Delta\mathbf{u}$. Accordingly, Eq. (B9) is simplified as

$$\rho_0 \frac{\partial \mathbf{u}_d}{\partial t} + \nabla p_d + \nabla\left(\frac{\rho_0 + \rho_d}{2}\mathbf{u}_d^2 - \frac{p_d^2}{2\rho_0 c_0^2}\right)$$

$$= \left(\frac{1}{3}\mu + \mu_B\right)\nabla(\nabla \cdot \mathbf{u}_d) + \mu\Delta\mathbf{u}_d. \quad (B11)$$

Here, we are considering a small nonlinearity case so that the dynamic fluctuation terms are not large. Thus, the third-order fluctuating term $\nabla(\rho_d\mathbf{u}_d^2/2)$ can be omitted as

$$\rho_0 \frac{\partial \mathbf{u}_d}{\partial t} + \nabla p_d + \nabla\left(\frac{\rho_0}{2}\mathbf{u}_d^2 - \frac{p_d^2}{2\rho_0 c_0^2}\right)$$

$$= \left(\frac{1}{3}\mu + \mu_B\right)\nabla(\nabla \cdot \mathbf{u}_d) + \mu\Delta\mathbf{u}_d. \quad (B12)$$

As a result, the continuity, momentum, and state equations for nonlinear acoustic media with loss can be summarized as

$$\frac{\partial \rho_d}{\partial t} + \rho_0\nabla \cdot \mathbf{u}_d = \frac{p_d}{\rho_0 c_0^4}\frac{\partial p_d}{\partial t} - \frac{1}{c_0^2}\mathbf{u}_d \cdot \nabla p_d, \quad (B13)$$

$$\rho_0\ \frac{\partial \mathbf{u}_d}{\partial t} + \nabla p_d + \nabla\left(\frac{\rho_0}{2}\mathbf{u}_d^2 - \frac{p_d^2}{2\rho_0 c_0^2}\right)$$

$$= \left(\frac{1}{3}\mu + \mu_B\right)\nabla(\nabla \cdot \mathbf{u}_d) + \mu\Delta\mathbf{u}_d \quad (B14)$$

$$\rho_d \cong \frac{p_d}{c_0^2}\left[1 - (\beta - 1)\frac{p_d}{\rho_0 c_0^2}\right]. \quad (B15)$$

Now, let us combine all three equations to derive the nonlinear acoustic equation with loss. First, differentiating Eq. (B13) with respect to time gives

$$\frac{\partial^2 \rho_d}{\partial t^2} + \rho_0\frac{\partial}{\partial t}(\nabla \cdot \mathbf{u}_d) = \frac{\partial}{\partial t}\left(\frac{p_d}{\rho_0 c_0^4}\frac{\partial p_d}{\partial t} - \frac{1}{c_0^2}\mathbf{u}_d \cdot \nabla p_d\right). \quad (B16)$$

Also differentiate both sides in Eq. (B14) as

$$\rho_0\nabla \cdot \left(\frac{\partial \mathbf{u}_d}{\partial t}\right) + \Delta p_d + \Delta\left(\frac{\rho_0}{2}\mathbf{u}_d^2 - \frac{p_d^2}{2\rho_0 c_0^2}\right)$$

$$= \left(\frac{1}{3}\mu + \mu_B\right)\Delta(\nabla \cdot \mathbf{u}_d) + \mu\nabla \cdot \Delta\mathbf{u}_d \quad (B17)$$

or, from $\Delta(\nabla \cdot \mathbf{u}) = \nabla \cdot \Delta\mathbf{u}$,

$$\rho_0\nabla \cdot \left(\frac{\partial \mathbf{u}_d}{\partial t}\right) + \Delta p_d + \Delta\left(\frac{\rho_0}{2}\mathbf{u}_d^2 - \frac{p_d^2}{2\rho_0 c_0^2}\right)$$

$$= \left(\frac{4}{3}\mu + \mu_B\right)\Delta(\nabla \cdot \mathbf{u}_d). \quad (B18)$$

Subtracting Eq. (B16) from Eq. (B18) yields

$$\Delta p_d - \frac{\partial^2 \rho_d}{\partial t^2} + \Delta\left(\frac{\rho_0}{2}\mathbf{u}_d^2 - \frac{p_d^2}{2\rho_0 c_0^2}\right)$$

$$+ \frac{\partial}{\partial t}\left(\frac{p_d}{\rho_0 c_0^4}\frac{\partial p_d}{\partial t} - \frac{1}{c_0^2}\mathbf{u}_d \cdot \nabla p_d\right)$$

$$= \left(\frac{4}{3}\mu + \mu_B\right)\Delta(\nabla \cdot \mathbf{u}_d). \quad (B19)$$

Also, substituting Eq. (B15) into Eq. (B19) yields

$$\Delta p_d - \frac{\partial^2}{\partial t^2}\left[\frac{p_d}{c_0^2} - (\beta - 1)\frac{p_d^2}{\rho_0 c_0^4}\right] + \Delta\left(\frac{\rho_0}{2}\mathbf{u}_d^2 - \frac{p_d^2}{2\rho_0 c_0^2}\right)$$

$$+ \frac{\partial}{\partial t}\left(\frac{p_d}{\rho_0 c_0^4}\frac{\partial p_d}{\partial t} - \frac{1}{c_0^2}\mathbf{u}_d \cdot \nabla p_d\right)$$

$$= \left(\frac{4}{3}\mu + \mu_B\right)\Delta(\nabla \cdot \mathbf{u}_d). \quad (B20)$$

Equation (B20) can be rearranged as

$$\Delta p_d - \frac{1}{c_0^2}\frac{\partial^2 p_d}{\partial t^2} = (1 - \beta)\frac{1}{\rho_0 c_0^4}\frac{\partial^2 p_d^2}{\partial t^2} + \frac{\Delta p_d^2}{2\rho_0 c_0^2} - \frac{\rho_0}{2}\Delta\mathbf{u}_d^2$$

$$- \frac{p_d}{\rho_0 c_0^4}\frac{\partial^2 p_d}{\partial t^2} + \frac{\partial}{\partial t}\left(\frac{1}{c_0^2}\mathbf{u}_d \cdot \nabla p_d\right)$$

$$+ \left(\frac{4}{3}\mu + \mu_B\right)\Delta(\nabla \cdot \mathbf{u}_d). \quad (B21)$$

Here, we will use the following equations to simplify Eq. (B21) [25]:

$$\frac{p_d}{\rho_0 c_0^4} \frac{\partial^2 p_d}{\partial t^2} = \frac{1}{2\rho_0 c_0^4} \frac{\partial^2 p_d^2}{\partial t^2}, \tag{B22}$$

$$\mathbf{u}_d \cdot \nabla p_d = -\frac{\rho_0}{2} \frac{\partial \mathbf{u}_d^2}{\partial t}. \tag{B23}$$

From Eqs. (B22) and (B23), Eq. (B21) can be rewritten as

$$\Delta p_d - \frac{1}{c_0^2} \frac{\partial^2 p_d}{\partial t^2} = (1-\beta)\frac{1}{\rho_0 c_0^4}\frac{\partial^2 p_d^2}{\partial t^2} + \frac{\Delta p_d^2}{2\rho_0 c_0^2} - \frac{\rho_0}{2}\Delta \mathbf{u}_d^2$$
$$- \frac{1}{2\rho_0 c_0^4}\frac{\partial^2 p_d^2}{\partial t^2} - \frac{\rho_0}{2c_0^2}\frac{\partial^2 \mathbf{u}_d^2}{\partial t^2}$$
$$+ \left(\frac{4}{3}\mu + \mu_B\right)\Delta(\nabla \cdot \mathbf{u}_d). \tag{B24}$$

Also, one can rearrange the right-hand side terms with the following equations [25]:

$$\Delta \mathbf{u}_d^2 = \frac{1}{c_0^2}\frac{\partial^2 \mathbf{u}_d^2}{\partial t^2}, \tag{B25}$$

$$\Delta p_d = \frac{1}{c_0^2}\frac{\partial^2 p_d}{\partial t^2}. \tag{B26}$$

As a result,

$$\Delta p_d - \frac{1}{c_0^2}\frac{\partial^2 p_d}{\partial t^2} = \frac{\partial^2}{\partial t^2}\left[(1-\beta)\frac{p_d^2}{\rho_0 c_0^4} - \frac{\rho_0}{c_0^2}\mathbf{u}_d^2\right]$$
$$+ \left(\frac{4}{3}\mu + \mu_B\right)\Delta(\nabla \cdot \mathbf{u}_d). \tag{B27}$$

Finally, the following equations can further simplify the equations [25]:

$$\mathbf{u}_d^2 = \left(\frac{1}{\rho_0 c_0}p_d\right)^2, \tag{B28}$$

$$\nabla \cdot \mathbf{u}_d \approx -\frac{1}{\rho_0}\frac{\partial \rho_d}{\partial t}, \tag{B29}$$

$$\rho_d = \frac{p_d}{c_0^2}. \tag{B30}$$

As a result, Eq. (B27) leads to

$$\Delta p_d - \frac{1}{c_0^2}\frac{\partial^2 p_d}{\partial t^2} = -\frac{\beta}{\rho_0 c_0^4}\frac{\partial^2 p_d^2}{\partial t^2}$$
$$- \frac{1}{\rho_0 c_0^2}\left(\frac{4}{3}\mu + \mu_B\right)\Delta\frac{\partial p_d}{\partial t}. \tag{B31}$$

Equation (B31) is a final form of acoustic equation that includes both viscosity and nonlinearity.

[1] L. Caspani *et al.*, J. Opt. Soc. Am. B **28**, A67 (2011).

[2] P. J. Westervelt, J. Acoust. Soc. Am. **35**, 535 (1963).

[3] H. O. Berktay, J. Sound. Vib. **2**, 435 (1965).

[4] W.-S. Gan, J. Yang, and T. Kamakura, Appl. Acoust. **73**, 1211 (2012).

[5] H. Nomura, C. M. Hedberg, and T. Kamakura, Appl. Acoust. **73**, 1231 (2012).

[6] A. Moussatov, B. Castagnede, and V. Gusev, Phys. Lett. A **301**, 281 (2002).

[7] K. Y. Jhang, Int. J. Precis. Eng. Manuf. **10**, 123 (2009).

[8] E. C. Everbach, *Parameters of Nonlinearity of Acoustic Media* (John Wiley & Sons, New York, 1998).

[9] M. S. Kushwaha, P. Halevi, L. Dobrzynski, and B. Djafari-Rouhani, Phys. Rev. Lett. **71**, 2022 (1993).

[10] M. M. Sigalas and E. N. Economou, Solid State Commun. **86**, 141 (1993).

[11] A. Khelif, B. Aoubiza, S. Mohammadi, A. Adibi, and V. Laude, Phys. Rev. E **74**, 046610 (2006).

[12] A. Khelif, A. Choujaa, S. Benchabane, B. Djafari-Rouhani, and V. Laude, Appl. Phys. Lett. **84**, 4400 (2004).

[13] A. Khelif, B. Djafari-Rouhani, J. O. Vasseur, and P. A. Deymier, Phys. Rev. B **68**, 024302 (2003).

[14] N. Fang, D. Xi, J. Xu, M. Ambati, W. Srituravanich, C. Sun, and X. Zhang, Nat. Mater. **5**, 452 (2006).

[15] H. H. Huang and C. T. Sun, J. Mech. Phys. Solids **59**, 2070 (2011).

[16] H. H. Huang, C. T. Sun, and G. L. Huang, Int. J. Eng. Sci. **47**, 610 (2009).

[17] J. H. Oh, H. M. Seung, and Y. Y. Kim, Appl. Phys. Lett. **108**, 093501 (2016).

[18] J. H. Oh, Y. E. Kwon, H. J. Lee, and Y. Y. Kim, Sci. Rep. **6**, 23630 (2016).

[19] C. Monat, M. De Sterke, and B. J. Eggleton, J. Opt. **12**, 104003 (2010).

[20] T. Baba, Nat. Photonics **2**, 465 (2008).

[21] C. Monat, B. Corcoran, M. Ebnali-Heidari, C. Grillet, B. J. Eggleton, T. P. White, L. O'Faolain, and T. F. Krauss, Opt. Express **17**, 2944 (2009).

[22] Y. A. Vlasov, M. O'Boyle, H. F. Hamann, and S. J. McNab, Nature **438**, 65 (2005).

[23] T. F. Krauss, J. Phys. D **40**, 2666 (2007).

[24] M. D. Settle, R. J. P. Engelen, M.Salib, A. Michaeli, L. Kuipers, and T. F. Krauss, Opt. Express **15**, 219 (2007).

[25] I. Shevchenko and B. Kaltenbacher, J. Comput. Phys. **302**, 200 (2015).

[26] J. J. Rushchitsky, *Nonlinear Elastic Waves in Materials* (Springer International Publishing, Heidelberg, 2014), p. 124.

[27] Z. Liang and J. Li, Phys. Rev. Lett. **108**, 114301 (2012).

[28] Y. Li, B. Liang, X. Tao, X. F. Zhu, X. Y. Zou, and J. C. Cheng, Appl. Phys. Lett. **101**, 233508 (2012).

[29] Y. Li, B. Liang, X. Y. Zou, and J. C. Cheng, Appl. Phys. Lett. **103**, 063509 (2013).

[30] Z. Liang, T. Feng, S. Lok, F. Liu, and K. Ng, Sci. Rep. **3**, 1614 (2013).

[31] K. Song, K. Kim, S. Hur, J. H. Kwak, J. Park, J. R. Yoon, and J. Kim, Sci. Rep. **4**, 7421 (2014).

[32] R. Khajehtourian and M. I. Hussein, AIP Adv. **4**, 124308 (2014).

[33] R. K. Narisetti, M. Ruzzene, and M. J. Leamy, Wave Motion **49**, 394 (2012).

[34] K. Manktelow, M. J. Leamy, and M. Ruzzene, Wave Motion **50**, 494 (2013).

[35] B. H. Song and J. S. Bolton, J. Acoust. Soc. Am. **107**, 1131 (2000).

[36] A. D. Pierce, *Acoustics: An Introduction to its Physical Principles and Applications* (McGraw-Hill, New York, 1981).

[37] G. Hernandez, *Fabry-Perot Interferometers* (Oxford University Press, Oxford, 1986).

[38] G. Theocharis, O. Richoux, V. R. Garca, A. Merkel, and V. Tournat, New. J. Phys. **16**, 093017 (2014).

[39] B. Witschas, M. O. Vieites, E. J. van Duijn, O. Reitebuch, W. van de Water, and W. Ubachs, Appl. Opt. **49**, 4217 (2010).

[40] D. T. Blackstock, *Fundamentals of Physical Acoustics* (John Wiley & Sons, New York, 2000).

[41] M. F. Hamilton and D. T. Blackstock, *Nonlinear Acoustics* (Academic, San Diego, CA, 1998).